Accurate estimation of cell composition in bulk expression through robust integration of single-cell information

Brandon Jew[1]*, Marcus Alvarez[2]*, Elior Rahmani[3], Zong Miao[1,2], Arthur Ko[2], Jae Hoon Sul[1,4], Kirsi H. Pietiläinen[5,6], Päivi Pajukanta[1,2,7]**, Eran Halperin[1,2,3]**

[1] Bioinformatics Interdepartmental Program, UCLA, Los Angeles, CA, USA, 90095

[2] Department of Human Genetics, David Geffen School of Medicine at UCLA, Los Angeles, CA, USA, 90095

[3] Computer Science Department in the School of Engineering, UCLA, Los Angeles, CA, USA, 90095

[4] Department of Psychiatry and Biobehavioral Sciences, UCLA, Los Angeles, CA, USA 90095

[5] Obesity Research Unit, Research Program for Clinical and Molecular Metabolism, University of Helsinki, Helsinki, Finland, 00014

[6] Obesity Center, Endocrinology, Abdominal Center, Helsinki University Central Hospital and University of Helsinki, Helsinki, Finland, 00260

[7] Institute for Precision Health, David Geffen School of Medicine at UCLA, Los Angeles, CA, USA, 90095

* These authors contributed equally to this work.

** Co-corresponding authors

Abstract

We present Bisque, a tool for estimating cell type proportions in bulk expression. Bisque implements a regression-based approach that utilizes single-cell RNA-seq (scRNA-seq) data to generate a reference expression profile and learn gene-specific bulk expression transformations to robustly decompose RNA-seq data. These transformations significantly improve decomposition performance compared to existing methods when there is significant technical variation in the generation of the reference profile and observed bulk expression. Importantly, compared to existing methods, our approach is extremely efficient, making it suitable for the analysis of large genomic datasets that are becoming ubiquitous. When applied to subcutaneous adipose and dorsolateral prefrontal cortex expression datasets with both bulk RNA-seq and single-nucleus RNA-seq (snRNA-seq) data, Bisque was able to replicate previously reported associations between cell type proportions and measured phenotypes across abundant and rare cell types. Bisque requires a single-cell reference dataset that reflects physiological cell type composition and can further leverage datasets that includes both bulk and single cell measurements over the same samples for improved accuracy. We further propose an additional mode of operation that merely requires a set of known marker genes. Bisque is available as an R package at: https://github.com/cozygene/bisque.

Introduction

Bulk RNA-seq experiments typically measure total gene expression from heterogeneous tissues, such as tumor and blood samples[1,2]. Variability in cell type composition can significantly confound analyses of these data, such as in identification of expression quantitative trait loci (eQTLs) or differentially expressed genes[3]. Cell type heterogeneity may also be of interest in profiling changes in tissue composition associated with disease, such as cancer[4] or diabetes[5]. In addition, measures of cell composition can be leveraged to identify cell-specific eQTLs[6,7] or differential expression[6] from bulk data.

Traditional methods for determining cell type composition, such as immunohistochemistry or flow cytometry, rely on a limited set of molecular markers and lack in scalability relative to the current rate of data generation[8]. Single-cell technologies provide a high-resolution view into cellular heterogeneity and cell type-specific expression[9–11]. However, these experiments remain costly and noisy compared to bulk RNA-seq[12]. Collection of bulk expression data remains an attractive approach for identifying population-level associations, such as differential expression regardless of cell type specificity. Moreover, many bulk RNA-seq studies that have been performed in recent years resulted in a large body of data that is available public databases such as dbGAP and GEO. Given the wide availability of these bulk data, the estimation of cell type proportions, often termed decomposition, can be used to extract large-scale cell type specific information.

There exist a number of methods for decomposing bulk expression, many of which are regression-based and leverage cell type-specific expression data as a reference profile[13]. CIBERSORT[14] is a SVM-regression based approach, originally designed for microarray data, that utilizes a reference generated from purified cell populations. A major limitation of this approach is the reliance on sorting cells to estimate a reference gene expression panel. BSEQ-sc[15] instead generates a reference profile from single-cell expression data that is used in the CIBERSORT model. MuSiC[16] also leverages single-cell expression as a reference, instead using a weighted non-negative least squares regression (NNLS) model for decomposition, with improved performance over BSEQ-sc in several datasets.

The distinct nature of the technologies used to generate bulk and single-cell sequencing data may present an issue for decomposition models that assume a direct proportional relationship between the single-cell-based reference and observed bulk mixture. For example, the capture of mRNA and chemistry of library preparation can differ significantly between bulk tissue and single-cell RNA-seq methods, as well as between different single-cell technologies[17,18]. Moreover, some technologies may be measuring different parts of the transcriptome, such as nuclear pre-mRNA in single-nucleus RNA-seq (snRNA-seq) experiments as opposed to cellular and extra-cellular mRNA observed in traditional bulk RNA-seq experiments. As we show later, these differences may introduce gene-specific biases that break down the correlation between cell type-specific and bulk tissue measurements. Thus, while single-cell RNA-seq technologies have provided unprecedented resolution in identifying expression profiles of cell types in heterogeneous tissues, these profiles generally may not follow the direct proportionality assumptions of regression-based methods, as we demonstrate here.

We present Bisque, a highly efficient tool to measure cellular heterogeneity in bulk expression through robust integration of single-cell information, accounting for biases introduced in the single-cell sequencing protocols. The goal of Bisque is to integrate the different chemistries/technologies of single-cell and bulk tissue RNA-seq to estimate cell type proportions from tissue-level gene expression measurements across a larger set of samples. Our reference-based model decomposes bulk samples using a single-cell-based reference profile and, while not required, can leverage single-cell and bulk measurements for the same samples for further improved decomposition accuracy. This approach employs gene-specific transformations of bulk expression to account for biases in sequencing technologies as described above. When a reference profile is not available, we propose BisqueMarker, a semi-supervised model that extracts trends in cellular composition from normalized bulk expression samples using only cell-specific marker genes that could be obtained using single cell data. We demonstrate using simulated and real datasets from brain and adipose tissue that our method is significantly more accurate than existing methods. Furthermore, it is extremely efficient, requiring seconds in cases where other methods require hours; thus, it is scalable to large genomic datasets that are now becoming available.

Results

Method overview (Bisque)

A graphical overview of Bisque is presented in Figure 1. Our reference-based decomposition model requires bulk RNA-seq counts data and a reference dataset with read counts from single-cell RNA-seq. In addition, the single-cell data should be labeled with cell types to be quantified. A reference profile is generated by averaging read count abundances within each cell type in the single-cell data. Given both the reference, our method learns gene-specific transformations of the bulk data to account for technical biases between the sequencing technologies. Bisque can then estimate cell proportions from the bulk RNA-seq data using the reference and the transformed bulk expression data using non-negative least-squares (NNLS) regression.

Evaluation of decomposition performance in human adipose tissue

We applied our method to 106 bulk RNA-seq subcutaneous adipose tissue samples collected from both lean and obese individuals, where 6 samples have both bulk RNA-seq and snRNA-seq data available (Table 1). Adipose tissue consists of several cell types, including adipocytes which are expected to be the most abundant population. Adipose tissue also contains structural cell types (i.e. fibroblasts and endothelial cells) and immune cells (i.e. macrophages and T cells)[19]. These 5 cell type populations were identified from the snRNA-seq data (Supplementary Fig. 1a).

We observed significant biases between the snRNA-seq and bulk RNA-seq data in samples that had both data available. We found that the linear relationship between the pseudo-bulk (summed snRNA-seq reads across cells) and the true bulk expression varied significantly by each gene (Fig. 2a). Specifically, we observed best fit lines relating these expression levels between technologies with a mean slope of roughly 0.30 and a variance in slope of 5.67. In our model, a slope of 1 would indicate no bias between technologies. We further investigated whether gene expression differences between the bulk and snRNA-seq were the same across individuals and experiments. Comparing log-ratios of RNA-seq to snRNA-seq expression levels, we found that the majority of gene biases were preserved across individuals, tissues, and experiments (R=0.75 across experiments) (Supplementary Fig. 3), providing evidence that technological differences drive consistent gene expression differences across bulk and snRNA-seq methods.

We performed simulations based on the adipose snRNA-seq data to demonstrate the effect of technology-based biases between the reference profile and bulk expression on decomposition performance. In these analyses, we benchmarked Bisque and three existing methods (MuSiC, BSEQ-sc, and CIBERSORT). Briefly, we simulated bulk expression for 6 individuals by summing the observed snRNA-seq read counts. To model discordance between the reference and bulk, we applied gene-specific linear transformations of the simulated bulk expression. For each gene, the coefficient and intercept of the linear transformation were sampled from half-normal distributions with increasing variance. In this model, a higher variance corresponds to a larger bias between sequencing experiments. While these transformations closely mirrored the Bisque decomposition model, they utilized the true snRNA-seq counts for each individual whereas Bisque learned these transformations using the reference profile generated from averaging these counts across all cells. Hence, this simulation framework introduced additional noise that Bisque does not entirely model. We evaluated decomposition performance by comparing proportion estimates to the proportions observed in the snRNA-seq data in terms of global Pearson correlation (R) and root mean squared deviation (RMSD). Due to the small number of samples, we applied leave-one-out cross-validation to predict the cell composition of each individual using the remaining snRNA-seq samples as training data for each method. In these simulations, Bisque remained robust (R ≈ 0.85, RMSD ≈ 0.07) at higher levels of simulated bias between the bulk and snRNA-seq-based reference (Fig. 2b).

Next, we performed this cross-validation benchmark on the observed bulk RNA-seq data for these 6 individuals and found that Bisque (R = 0.923, RMSD = 0.074) provided significantly improved global accuracy in detecting each cell type over existing methods (Table 2, Supplementary Fig. 1b). MuSiC (R = -0.111, RMSD = 0.427), BSEQ-sc (R = -0.113, RMSD = 0.432), and CIBERSORT (R = -0.131, RMSD = 0.416) severely underestimated the proportion of adipocytes (the most abundant population in adipose tissue) while overestimating the endothelial cell fraction. We also benchmarked CIBERSORTx[20], which employs a batch correction mode to account for biases in sequencing technologies. While CIBERSORTx (R = 0.687, RMSD = 0.099) outperformed existing methods, Bisque provided improved accuracy. It should be noted that cell-specific accuracy is more informative than global R and RMSD; however, these small sample sizes did not provide robust measures of within-cell-type performance in this cross-validation framework (Supplementary Fig. 1c). We were able to slightly improve the number of detected cell populations by MuSiC, BSEQ-sc, and CIBERSORT when we considered only snRNA-seq reads aligning to exonic regions of the transcriptome, indicating that intronic reads introduced increasing discrepancy between snRNA-seq and bulk RNA-seq in the context of decomposition. However, given that a significant portion of the nuclear transcriptome consists of pre-mRNA, this filtering process removed over 40 percent of cells detected in the snRNA-seq data. Moreover, Bisque provided improved accuracy over existing methods using this exonic subset of the snRNA-seq data (Supplementary Fig. 1d).

We then applied these decomposition methods to the remaining 100 bulk samples and found that the distribution of cell proportion estimates produced by Bisque were most concordant with the expected distribution inferred from the limited number of snRNA-seq samples and previously reported proportions[21,22] (Fig. 3a). While these benchmarks provided a measure of calibration (i.e. the ability to detect cell populations in expected ranges), they did not provide measurements of cell-specific proportion accuracy across individuals. In order to evaluate cell-specific accuracy, we replicated previously reported associations between cell proportions and measured phenotypes. Specifically, we compared cell proportion estimates from each method to body mass index (BMI) and Matsuda index, a measure of insulin resistance. We measured the significance of these association accounting for age, age-squared, sex, and relatedness.

Obesity is associated with adipocyte hypertrophy, the expansion of the volume of fat cells[23]; thus, we expected a negative association between adipocyte proportion and BMI. Bisque, MuSiC and CIBERSORTx produced adipocyte proportion estimates that replicate this behavior, while BSEQ-sc and CIBERSORT were unable to detect this cell population (Fig. 3b). The adipocyte proportion estimates produced by Bisque ($p = 0.030$) and CIBERSORTx ($p = 0.001$) had a significant negative association with BMI (Supplementary Table 1a). In addition, macrophage abundance has been shown to increase in adipose tissue with higher levels of obesity, concomitant with a state of low grade inflammation[24]. Each method detected macrophage populations that positively associated with BMI; however, only Bisque ($p < 0.001$), BSEQ-sc ($p = 0.004$) and CIBERSORTx ($p = 0.049$) reached significance (Supplementary Table 1b).

T cells were the least abundant cell type population identified from the snRNA-seq data, constituting around 4 percent of all sequenced nuclei. The abundance of T cells has been observed to positively correlate with insulin resistance[25]. Thus, we compared decomposition estimates for T cell proportions to Matsuda index. As a lower Matsuda index indicates higher insulin resistance, we expect a negative association between T cell proportion and Matsuda index. Proportion estimates produced by Bisque and CIBERSORTx followed this trend while the remaining existing methods did not identify T cells in the bulk samples (Fig. 3c). We found this association significant for Bisque ($p < 0.001$) and CIBERSORTx ($p = 0.047$) (Supplementary Table 1c) after correcting for diabetes status, since Matsuda index may not be informative in these individuals[26].

Evaluation of decomposition performance in human dorsolateral prefrontal cortex tissue

We also benchmarked these decomposition methods using expression data collected from the dorsolateral prefrontal cortex (DLPFC). This dataset was generated by the Rush Alzheimer's Disease (AD) Center[27] and includes 636 postmortem bulk RNA-seq samples. Both bulk RNA-seq and snRNA-seq data were collected from 8 of the individuals (Table 1). Using the same pipeline we used to process the adipose dataset, we identified 11 clusters: 3 neuronal subtypes, 2 interneuronal subtypes, 2 astrocyte subtypes, oligodendrocytes, oligodendrocyte progenitor cells, and microglia (Supplementary Fig. 2a). We observed a higher overlap in marker genes for these clusters than in those identified in the adipose dataset (average of 10% of marker genes shared between clusters in DLPFC compared to 3% in adipose) (Supplementary Fig. 4a-b)

We again applied leave-one-out cross-validation on the 8 individuals with both RNA-seq and snRNA-seq data available. In this example, randomly sampled 25% of the nuclei in the snRNA-seq data to accommodate CIBERSORTx (which is currently web-based and restricts the size of files that can be processed). Bisque was able to detect each cell population identified from the snRNA-seq data with high global accuracy (R=0.924, RMSD=0.029) while MuSiC (R = -0.192, RMSD = 0.173), BSEQ-sc (R = 0.098, RMSD = 0.120), and CIBERSORT (R = -0.281, RMSD = 0.197) did not detect a number of cell populations (Table 3, Supplementary Fig. 2b, Supplementary Fig. 2c). Bisque also provided higher accuracy than CIBERSORTx (R = 0.671, RMSD = 0.070). However, we found that the performance of the existing methods improved when estimates with subtypes were summed together (Supplementary Fig. 2d). While each method was able to quantify major cell populations after merging subtypes, Bisque was able to distinguish between these closely related cell populations. Interestingly, we found that in both adipose and DLPFC, endothelial cell proportions were overestimated by each of the existing methods.

We applied these decomposition methods to the remaining 628 individuals and compared the distribution of estimates to the proportions observed in the 8 snRNA-seq samples. We found that Bisque was able to detect each cell population and produced estimates that were closest in mean to the snRNA-seq observations (Fig. 4a). The increased accuracy of Bisque over existing methods persisted when we merged closely related subtypes (Supplementary Fig. 2e). Moreover, immunohistochemistry (IHC) analyses on a 70 of these samples found similar proportions of major cell populations[28], confirming the relative accuracy of snRNA-seq based estimates of cell proportions.

Again, to determine cell-specific decomposition accuracy, we replicated known associations between cell type proportions and measured phenotypes in the 628 individuals. For these analyses, we compared cell proportion estimates to each individual's Braak stage and physician cognitive diagnostic category at time of death. Braak stage is a semiquantitative measure of neurofibrillary tangles, ranging in value from 0 to 5 with increasing severity. The cognitive diagnostic category provides a semiquantitative measure of dementia severity, where a code of 1 indicates no cognitive impairment and 5 indicates a confident diagnosis of AD by physicians. We accounted for age, age-squared, and sex to determine the significance of these associations.

Neuronal death is a hallmark symptom of AD[29]. Therefore, we expected to find a negative association between cognitive diagnosis and neuron proportion. We found that each decomposition method provides estimates of total neuron proportion that tend to decrease with cognitive diagnostic category (Fig. 4b). Each method generates proportions with negative association with cognitive diagnosis. Each method, excluding BSEQ-sc, reached significance in this model ($p \leq 0.003$ for each method) (Supplementary Table 2a). As another example, we compared each individual's Braak stage to their estimated proportion of microglia, a relatively small cell population that constituted roughly 5 percent of the sequenced nuclei. Microglia activation has been observed to increase with AD severity[30]. We used Braak stage as a proxy for AD severity and expected a positive association between microglia proportion and Braak stage. Bisque and MuSiC provided estimates that follow this expected trend (Fig. 4c). Only Bisque produced estimates with a significant positive association ($p = 0.001$) (Supplementary Table 2b). Interestingly, we observe a decrease in microglia proportions estimated by Bisque in Braak stage 6 individuals which has been previously observed in AD patients[31].

Runtime comparisons of reference-based decomposition methods

Given the large amounts of transcriptomic data that are becoming available, we also benchmarked these decomposition methods in terms of runtime. In the subcutaneous adipose dataset, which included 100 bulk RNA-seq samples and 6 snRNA-seq samples with about 1,800 nuclei sequenced per individual, Bisque was able to estimate cell proportions efficiently compared to existing methods. Bisque (1 second) and MuSiC (1 second) provided decomposition estimates faster than BSEQ-sc (26 seconds), CIBERSORT (27 seconds), and CIBERSORTx (389 seconds) (Fig. 5a). Bisque also provided improved efficiency in processing the reduced DLPFC dataset, which included 628 bulk RNA-seq samples and 8 snRNA-seq samples with around 2,125 nuclei per individual. Bisque (4 seconds) and MuSiC (10 seconds) estimated cell proportions relatively quickly compared to BSEQ-sc (273 seconds), CIBERSORT (298 seconds), and CIBERSORTx (6,566 seconds) (Fig. 5b).

Marker-based decomposition using known cell type marker genes

While a reference profile from snRNA-seq can help to decompose bulk level gene expression, it may not be available for the same data set. The majority of bulk RNA-seq data sets do not have corresponding snRNA-seq data in the same set of individuals. However, marker gene information from prior experiments can still be applied to distinct expression data sets of the same tissue. The basis of most decomposition methods relies on the logic that as the proportion of a cell type varies across individuals, the expression of its marker genes will tend to correlate in the same direction as its cell type proportion. This linear co-variation can be captured in a principal components analysis (PCA). Under the same argument, the more cell type-specific a marker gene is, the more its expression will reflect its cell type proportion. These observations form the basis for BisqueMarker, a weighted PCA-based (wPCA) decomposition approach. Genes that are more specifically expressed within a cell type will provide more information than genes with shared expression across cell types. To estimate cell type proportions without the use of cell type-specific gene expression information, we applied wPCA to bulk-level adipose tissue expression.

For each cell type, we extracted the first PC from a wPCA of the expression matrix of its markers. The expression matrix was corrected for the first global expression PC as a covariate so that wPCA estimates would not reflect technical variation. We first confirmed that these genes were distinct across cell types. If 2 cell types share a high proportion of marker genes, the wPCA estimates from bulk RNA-seq will correlate highly. We then investigated whether the second or third PC could have represented cell type proportions. The percent of variance explained by the first PC was typically 30-60% across adipose cell types, and additionally, over 90% of the markers correlated in the same direction as the first PC. In contrast, roughly 50-70% of markers correlated in the same direction as the second or third PC. As performed for reference-based decomposition, we correlated phenotypes with cell type proportions estimated by BisqueMarker. We identified the same associations as with reference-based decomposition, demonstrating its validity when a reference is not available (Supplementary Table 1). Similarly, we observed the same trends between estimated cell type abundances and phenotypes as we did using our reference-based method in the DLPFC cohort (Supplementary Table 2).

Discussion

Bisque effectively leverages single-cell information to decompose bulk expression samples, outperforming existing methods in datasets with snRNA-seq data available. In simulations, we demonstrated that the decomposition accuracy of Bisque is robust to increasing variation between the generation of the reference profile and bulk expression, which is a significant issue when comparing snRNA-seq and bulk RNA-seq data. In observed bulk expression, our reference-based method accurately estimates cell proportions that are consistent with previously reported distributions and reliably detects rare cell types. We found that these estimates consistently follow expected trends with measured phenotypes, suggesting that cell-specific estimates of proportion are sufficiently accurate to extract relevant biological signals. In addition, differences in tissue structure can lead to significant differences in the quality of single-cell expression data[32]. We demonstrated the improved performance of our method in adipose and DLPFC, two distinct tissues, suggesting that Bisque is robust across different tissue types.

The cell type proportion estimates determined by Bisque may be utilized to effectively identify cell-type-specific interactions, such as expression quantitative trait loci (eQTLs), and adjust for confounding effects from variability in cell populations. With this reference-based approach, single-cell sequencing of a subset of samples from large-scale bulk expression cohorts can provide high power to detect cell-specific associations in complex phenotypes and diseases.

However, we note that there are limitations to this reference-based method that users should consider. First, if the number of individuals with single-cell data available is small, the reference profile and gene-specific transformations may become unreliable. In addition, a key assumption of our transformation framework is that single-cell based estimates of cell proportions accurately reflect the true proportions we wish to estimate. Given that snRNA-seq can provide less bias in isolating specific cell types compared to scRNA-seq[33,34], we expect our reference-based method to have more significant improvement over existing methods using these data. Nevertheless, the accuracy of Bisque may decrease if the proportion of cell types captured by single-cell experiments differs significantly from the true physiological distributions. Our results demonstrate that even with these limitations, Bisque can be used to provide cell-type specific biological insight in relevant datasets.

In cases where these described issues may be significant, BisqueMarker provides cell type abundance estimations using only known marker genes. While this reference-free method may be less accurate than reference-based methods, it does not depend on single-cell based estimates of cell proportions or expression profiles, but rather on the fact that the expression in certain genes differs across different cell types; moreover, this method also does not model explicitly the expression level, and it is thus robust to biases in the single cell sequencing protocol. We found that BisqueMarker estimates followed expected trends with measured phenotypes; however, it should be noted that this method estimates relative differences in abundances that cannot be compared across cell types. Also, given the semi-supervised nature of this method, these cell type abundance estimates may include signals from technical or other biological variation in the data. Therefore, we highly suggest applying this method to data that is properly normalized with sources of undesired variation removed.

Methods

Processing bulk expression data

Paired-end reads were aligned with STAR v2.5.1 using default options. Gene counts were quantified using featureCounts v1.6.3. For featureCounts, fragments were counted at the gene-name level. Alignment and gene counts were generated against the GRCh38.p12 genome assembly. STAR v2.5.1 and GRCh38.p12 were included with CellRanger 3.0.2, which was used to process the single-nucleus data.

Processing single-nucleus expression data

Reads from single nuclei sequenced on the 10x Genomics Chromium platform were aligned and quantified using the CellRanger 3.0.2 count function against the GRCh38.p12 genome assembly. To account for reads aligning to both exonic and intronic regions, each gene transcript in this reference assembly was relabeled as an exon since CellRanger counts exonic reads only. We perform this additional step since snRNA-seq captures both mature mRNA and pre-mRNA, the latter of which includes intronic regions.

After aggregating each single-nucleus sample with the CellRanger aggr function, the full dataset was processed using Seurat v3.0.0[35]. The data were initially filtered for genes expressed in at least 3 cells and filtered for cells with reads quantified for between 200 and 2,500 genes. We further filtered for cells that had percentage of counts coming from mitochondrial genes less than or equal to 5 percent. The data were normalized, scaled, and corrected for mitochondrial read percentages with sctransform v0.2.0[36] using default options.

To identify clusters, Seurat employs a shared nearest neighbor approach. We identified clusters using the top 10 principal components of the processed expression data with resolution set at 0.2. The resolution parameter controls the number of clusters that will be identified, and suggested values vary depending on the size and quality of the dataset. We chose a value that produced 6 clusters in the adipose dataset and 13 clusters in the DLPFC dataset and visualized the clustering results with UMAP[37].

Marker genes were identified by determining the average log-fold change of expression of each cluster compared to the rest of the cells. We identified marker genes as those with an average log-fold change above 0.25. The significance of the differential expression of these genes was determined using a Wilcoxon rank sum test. Only genes that were detected in at least 25 percent of cells were considered. Clusters with many mitochondrial genes as markers (nine genes detected in both datasets) were removed from both datasets. In addition, a cluster with only three marker genes was removed from the DLPFC datasets. Finally, we remove mitochondrial genes from the list of marker genes for decomposition as we assume reads aligning to the mitochondrial genome originate from extra-nuclear RNA in the snRNA-seq dataset (targeting nuclear RNA).

Clusters were labeled by considering cell types associated with the identified marker genes. Marker genes were downloaded from PanglaoDB[38] and filtered for entries validated in human cells. For each gene, we count the possible cell type labels. Each cluster was labeled as the most frequent cell type across all of its marker genes, with each label associated with a gene weighted by the average log-fold change. If multiple clusters shared a cell type label, we consider each cluster a subtype of this label.

Exon-aligned reads were processed in the same exact procedure but snRNA-seq data was aligned to just exonic regions. Cluster names were manually changed for both datasets when aligned to exons to match the clusters from intronic reads as well. Specifically, for clusters identified in the exonic data not found in the full data, we relabeled as the label with the highest score found in the full data. These relabeled clusters were similar in proportion to the corresponding cluster in the full dataset.

Learning a single-cell based reference and bulk transformation for reference-based decomposition

We assume that only a subset of genes are relevant for estimating cell type composition. For the adipose and DLPFC datasets, we selected the marker genes identified by Seurat as described previously. Moreover, we filter out genes with zero variance in the single-cell data, unexpressed genes in the bulk expression, and mitochondrial genes. We convert the remaining gene counts to counts-per-million to account for variable sequencing depth. For m genes and k cell types, a reference profile $Z \in \mathbb{R}^{m \times k}$ is generated by averaging relative abundances within each cell type across the entire single-cell dataset.

Though there is a strong positive correlation between bulk and single-cell based pseudo-bulk (summed single-cell counts) expression data, we observe that the relationship is not one-to-one and varies between genes. This behavior indicates that the distribution of observed bulk expression may significantly differ from the distribution of the single-cell profile weighted by cell proportions. We propose transforming the bulk data to maximize the global linear relationship across all genes for improved decomposition. Our goal is to recover a one-to-one relationship between the transformed bulk and expected convolutions of the reference profile based on single-cell based estimates of cell proportions. This transformed bulk expression better satisfies the assumptions of regression-based approaches under sum-to-one constraints.

Cell type proportions $p \in \mathbb{R}^{k \times n'}$ are determined by counting the cells with each label in the single-cell data for n' individuals. Given these proportions and the reference profile Z, we calculate the pseudo-bulk for the single-cell samples as $Y = Zp$, where $Y \in \mathbb{R}^{m \times n'}$. For each gene j, our goal is to transform the observed bulk expression across all n bulk samples $X_j \in \mathbb{R}^n$ to match the mean and variance of $Y_j \in \mathbb{R}^{n'}$; hence, the transformation of X_j will be a linear transformation.

If individuals with both single-cell and bulk expression are available, we fit a linear regression model to learn this transformation. Let X'_j denote the expression values for these n' overlapping individuals. We fit the following model (with an intercept) and apply the model to the remaining bulk samples as our transformation:

$$Y_j = \beta_j X'_j + \epsilon_j$$

If there are no single-cell samples that have bulk expression available, we assume that the observed mean of Y_j is the true mean of our goal distribution for the transformed X_j. We further assume that the sample variance observed in Y_j is larger than the true variance of the goal distribution, since the number of single-cell samples is typically small. We use a shrinkage estimator of the sample variance of Y_j that minimizes the mean squared error and results in a smaller variance than the unbiased estimator:

$$\hat{\sigma}_j^2 = \frac{1}{n'+1} \sum_{i=1}^{n'} (Y_{i,j} - \bar{Y}_j)^2$$

We transform the remaining bulk as follows:

$$X_{j,transformed} = \frac{X_j - \bar{X}_j}{\sigma_{X_j}} \hat{\sigma}_j + \bar{Y}_j$$

where a bar indicates the mean value of the observed data and σ_{X_j} is the unbiased sample variance of X_j.

To estimate cell type proportions, we apply non-negative least squares regression with an additional sum-to-one constraint to the transformed bulk data. For individual i, we minimize the following with respect to the cell proportion estimate p_i:

$$\|Zp_i - X_{i,transformed}\|_2 \text{ s.t. } p_i \geq 0, \ \sum p_i = 1$$

Simulating bulk expression based on single-nucleus counts

We simulate the base bulk expression as the sum of all counts across cells/nuclei sequenced from an individual. To introduce gene-specific variation between the bulk and single-cell data, we sample a coefficient β_j and an intercept α_j from a half-normal (HN) distributions:

$$\beta_j \sim HN(1, \sigma)$$

$$\alpha_j \sim HN(0, \sigma)$$

where the variance of the HN distribution is $\sigma^2(1 - \frac{2}{\pi})$. At $\sigma = 0$, the base simulated bulk expression remains unchanged. We used a HN distribution to ensure coefficients and intercepts are positive. While our method can handle negative coefficients, this simulation model assumes expression levels have a positive correlation across technologies. We performed 10 replicates of this data-generating process at each σ in 0, 5, 10, 20. Decomposition performance on these data were measured in terms of global R and RMSD and plotted with 95% confidence intervals based on bootstrapping.

Determining significance of cell proportion associations with measured phenotypes

Reported associations were measured in terms of Spearman correlation. To determine the statistical significance of these associations while accounting for possible confounding factors, we applied two approaches. For the adipose dataset, which consisted entirely of twin pairs, we applied a linear mixed-effects model (R nlme package) with random effects accounting for family. For the DLPFC dataset, we assumed individuals were unrelated and fit a simple linear model (R base package). In each model, we include cell type proportion, age, age-squared, and sex as covariates. We introduced an additional covariate for diabetes status when regressing Matsuda index due to a known significant association between these two variables. We test whether the cell proportion effect estimates deviate significantly from 0 using a t-test. Each R method implements the described model fitting and significance testing.

Estimating relative cellular heterogeneity with a semi-supervised weighted PCA model

In order to estimate cell type proportions across individuals without the use of a cell type-specific gene expression panel as reference, we use a weighted PCA approach. BisqueMarker requires a set of marker genes for each cell type as well as the specificity of each marker determined by the fold change from a differential expression analysis. Typical single-cell RNA-seq workflows calculate marker genes and provide both p-values and fold changes, as in Seurat[35]. For each cell type, we take statistically significant marker genes (FDR < 0.05) ranked by p-value. A weighted PCA is calculated on the expression matrix using a subset of the marker genes by first scaling the expression matrix and multiplying each gene column by its weight (the log fold-change) XW, where X is the sample by gene expression matrix and W is a diagonal matrix with entries equal to log fold-change of the corresponding gene. The bulk expression X should be corrected for global covariates so that the proportion estimates do not reflect this global variation. The first PC calculated from XW is used as the estimate of the cell type proportion. This allows cell type-specific genes to be prioritized over more broadly expressed genes. Alternatively, if weights are not available, PCA can be run on the matrix X and the first PC can be used.

In order to select marker genes, we iteratively run the above PCA procedure on a specified range of markers (from 25 to 200) and calculate the ratio of the first eigenvalue to the second. We then select the number of marker genes to use that maximizes this ratio. This procedure is similar to other methods which select the number of markers to use by maximizing the condition number of the reference matrix[13].

References

1. Tomczak, K., Czerwińska, P. & Wiznerowicz, M. The Cancer Genome Atlas (TCGA): an immeasurable source of knowledge. *Contemp. Oncol.* **19**, A68–77 (2015).
2. GTEx Consortium. Human genomics. The Genotype-Tissue Expression (GTEx) pilot analysis: multitissue gene regulation in humans. *Science* **348**, 648–660 (2015).
3. Bruning, O. *et al.* Confounding Factors in the Transcriptome Analysis of an In-Vivo Exposure Experiment. *PLoS One* **11**, e0145252 (2016).
4. Fridman, W. H., Pagès, F., Sautès-Fridman, C. & Galon, J. The immune contexture in human tumours: impact on clinical outcome. *Nat. Rev. Cancer* **12**, 298–306 (2012).
5. Rahier, J., Goebbels, R. M. & Henquin, J. C. Cellular composition of the human diabetic pancreas. *Diabetologia* **24**, (1983).
6. Shen-Orr, S. S. *et al.* Cell type–specific gene expression differences in complex tissues. *Nature Methods* **7**, 287–289 (2010).
7. Westra, H.-J. *et al.* Cell Specific eQTL Analysis without Sorting Cells. *PLoS Genet.* **11**, e1005223 (2015).
8. Hu, P., Zhang, W., Xin, H. & Deng, G. Single Cell Isolation and Analysis. *Frontiers in Cell and Developmental Biology* **4**, (2016).
9. Zheng, G. X. Y. *et al.* Massively parallel digital transcriptional profiling of single cells. *Nat. Commun.* **8**, 14049 (2017).
10. Tasic, B. *et al.* Shared and distinct transcriptomic cell types across neocortical areas. *Nature* **563**, 72–78 (2018).
11. Macosko, E. Z. *et al.* Highly Parallel Genome-wide Expression Profiling of Individual Cells

Using Nanoliter Droplets. *Cell* **161**, 1202–1214 (2015).

12. Wang, J. *et al.* Gene expression distribution deconvolution in single-cell RNA sequencing. *Proc. Natl. Acad. Sci. U. S. A.* **115**, E6437–E6446 (2018).
13. Mohammadi, S., Zuckerman, N., Goldsmith, A. & Grama, A. A Critical Survey of Deconvolution Methods for Separating Cell Types in Complex Tissues. *Proceedings of the IEEE* **105**, 340–366 (2017).
14. Newman, A. M. *et al.* Robust enumeration of cell subsets from tissue expression profiles. *Nat. Methods* **12**, 453–457 (2015).
15. Baron, M. *et al.* A Single-Cell Transcriptomic Map of the Human and Mouse Pancreas Reveals Inter- and Intra-cell Population Structure. *Cell Syst* **3**, 346–360.e4 (2016).
16. Wang, X., Park, J., Susztak, K., Zhang, N. R. & Li, M. Bulk tissue cell type deconvolution with multi-subject single-cell expression reference. *Nat. Commun.* **10**, 380 (2019).
17. Ziegenhain, C. *et al.* Comparative Analysis of Single-Cell RNA Sequencing Methods. *Mol. Cell* **65**, 631–643.e4 (2017).
18. La Manno, G. *et al.* RNA velocity of single cells. *Nature* **560**, 494–498 (2018).
19. Esteve Ràfols, M. Adipose tissue: cell heterogeneity and functional diversity. *Endocrinol. Nutr.* **61**, 100–112 (2014).
20. Newman, A. M. *et al.* Determining cell type abundance and expression from bulk tissues with digital cytometry. *Nat. Biotechnol.* (2019). doi:10.1038/s41587-019-0114-2
21. Rosen, E. D. & Spiegelman, B. M. What We Talk About When We Talk About Fat. *Cell* **156**, 20–44 (2014).
22. Glastonbury, C. A., Alves, A. C., Moustafa, J. E.-S. & Small, K. S. Cell-type heterogeneity

in adipose tissue is associated with complex traits and reveals disease-relevant cell-specific eQTLs. *Am. J. Hum. Genet.* (2019). doi:10.1016/j.ajhg.2019.03.025

23. Spalding, K. L. *et al.* Dynamics of Fat Cell Turnover in Humans. *Obstetrical & Gynecological Survey* **63**, 577–578 (2008).
24. Weisberg, S. P. *et al.* Obesity is associated with macrophage accumulation in adipose tissue. *Journal of Clinical Investigation* **112**, 1796–1808 (2003).
25. McLaughlin, T. *et al.* T-Cell Profile in Adipose Tissue is Associated with Insulin Resistance and Systemic Inflammation in Humans. *Arterioscler. Thromb. Vasc. Biol.* **34**, 2637 (2014).
26. Gutch, M., Kumar, S., Razi, S., Gupta, K. & Gupta, A. Assessment of insulin sensitivity/resistance. *Indian Journal of Endocrinology and Metabolism* **19**, 160 (2015).
27. Mostafavi, S. *et al.* A molecular network of the aging human brain provides insights into the pathology and cognitive decline of Alzheimer's disease. *Nat. Neurosci.* **21**, 811–819 (2018).
28. Patrick, E. *et al.* Deconvolving the contributions of cell-type heterogeneity on cortical gene expression. doi:10.1101/566307
29. Yankner, B. A. Mechanisms of Neuronal Degeneration in Alzheimer's Disease. *Neuron* **16**, 921–932 (1996).
30. Hansen, D. V., Hanson, J. E. & Sheng, M. Microglia in Alzheimer's disease. *J. Cell Biol.* **217**, 459–472 (2018).
31. Navarro, V. *et al.* Microglia in Alzheimer's Disease: Activated, Dysfunctional or Degenerative. *Frontiers in Aging Neuroscience* **10**, (2018).
32. Nguyen, Q. H., Pervolarakis, N., Nee, K. & Kessenbrock, K. Experimental Considerations for Single-Cell RNA Sequencing Approaches. *Front Cell Dev Biol* **6**, 108 (2018).

33. Wu, H., Kirita, Y., Donnelly, E. L. & Humphreys, B. D. Advantages of Single-Nucleus over Single-Cell RNA Sequencing of Adult Kidney: Rare Cell Types and Novel Cell States Revealed in Fibrosis. *J. Am. Soc. Nephrol.* **30**, 23–32 (2019).

34. Bakken, T. E. *et al.* Single-nucleus and single-cell transcriptomes compared in matched cortical cell types. *PLoS One* **13**, e0209648 (2018).

35. Butler, A., Hoffman, P., Smibert, P., Papalexi, E. & Satija, R. Integrating single-cell transcriptomic data across different conditions, technologies, and species. *Nat. Biotechnol.* **36**, 411–420 (2018).

36. Hafemeister, C. & Satija, R. Normalization and variance stabilization of single-cell RNA-seq data using regularized negative binomial regression. doi:10.1101/576827

37. McInnes, L., Healy, J., Saul, N. & Großberger, L. UMAP: Uniform Manifold Approximation and Projection. *Journal of Open Source Software* **3**, 861 (2018).

38. Franzén, O., Gan, L.-M. & Björkegren, J. L. M. PanglaoDB: a web server for exploration of mouse and human single-cell RNA sequencing data. *Database* **2019**, (2019).

Acknowledgements

We thank the individuals who participated in the Finnish twin study, as well as Jaakko Kaprio and Aila Rissanen for the contributions to the twin study. We also thank the UNGC sequencing core at UCLA for performing RNA sequencing. This study was funded by National Institutes of Health (NIH) grants HL-095056, HL-28481, and U01 DK105561. K.H.P. was supported by the Academy of Finland (272376, 266286, 314383, 315035), Finnish Medical Foundation, Finnish Diabetes Research Foundation, Novo Nordisk Foundation, Gyllenberg Foundation, Sigrid Juselius Foundation, Helsinki University Hospital Research Funds and University of Helsinki. The funders had no role in study design, data collection, and analysis, decision to publish, or preparation of the article. The results published here are in whole or in part based on data obtained from the AMP-AD Knowledge Portal (doi:10.7303/syn2580853). Study data were provided by the Rush Alzheimer's Disease Center, Rush University Medical Center, Chicago. Data collection was supported through funding by NIA grants P30AG10161, R01AG15819, R01AG17917, R01AG30146, R01AG36836, U01AG32984, U01AG46152, U01AG61356, the Illinois Department of Public Health, and the Translational Genomics Research Institute. B.J. was supported by the National Science Foundation Graduate Research Fellowship Program under Grant No. DGE-1650604. M.A. was supported by the HHMI Gilliam fellowship. Z.M was supported by the AHA grant 19PRE34430112. E.H., B.J., and E.R. were partially supported by the National Science Foundation (Grant No. 1705197).

Author Contributions

E.H. and P.P. conceived of and supervised the study. B.J. and M.A. developed the method and associated software as well as carried out experiments. K.H.P. provided the subcutaneous adipose samples. J.H.S. provided guidance on the analysis of the dorsolateral prefrontal cortex dataset. E.R., Z.M., and A.K. provided statistical and biological insight for the method validation. B.J., M.A., P.P. and E.H. wrote the manuscript with support from all authors.

Competing Interests

The authors declare no competing interests.

Tables

Tissue	**Number of Samples**	**Bulk RNA-seq platform**	**snRNA-seq platform**	**snRNA-seq samples**	**Total nuclei**	**Average nuclei per individual**	**Number of cell types**
Subcutaneous adipose	106	Illumina NovaSeq	10x Genomics Chromium	6	10,947	1,824	5
Dorsolateral prefrontal cortex	636	Illumina HiSeq	10x Genomics Chromium	8	68,028	8,503	11

Table 1: Summary of snRNA-seq and bulk expression datasets used for benchmarking Bisque and existing methods.

Method	**R**	**RMSD**
Bisque	**0.923 ± 0.064**	**0.074 ± 0.034**
CIBERSORTx	0.687 ± 0.450	0.099 ± 0.046
MuSiC	-0.111 ± 0.182	0.427 ± 0.058
BSEQ-sc	-0.113 ± 0.180	0.432 ± 0.058
CIBERSORT	-0.131 ± 0.176	0.416 ± 0.059

Table 2: Leave-one-out cross-validation in subcutaneous adipose using 6 samples with snRNA-seq and bulk RNA-seq data available. Proportions based on snRNA-seq were used as a proxy for the true proportions. Performance measured in Pearson correlation (R) and root-mean-square deviation (RMSD) across all 5 identified cell types in each sample. Reported values were averaged across the 6 samples with standard deviation indicated.

Method	**R**	**RMSD**
Bisque	**0.924 ± 0.062**	**0.029 ± 0.010**
CIBERSORTx	0.671 ± 0.153	0.070 ± 0.019
MuSiC	-0.192 ± 0.107	0.173 ± 0.013
BSEQ-sc	0.098 ± 0.216	0.120 ± 0.023
CIBERSORT	-0.281 ± 0.049	0.197 ± 0.012

Table 3: Leave-one-out cross-validation in dorsolateral prefrontal cortex using 8 samples with snRNA-seq and bulk RNA-seq data available. Proportions based on snRNA-seq were used as a proxy for the true proportions. Performance measured in Pearson correlation (R) and root-mean-square deviation across all 11 identified cell types in each sample. Reported values were averaged across the 8 samples with standard deviation indicated. We performed these experiments with 25% of the snRNA-seq data in order to accommodate the file size limit of the current web-based implementation of CIBERSORTx.

Supplementary Tables

a Association of adipocyte proportion estimates in adipose tissue with BMI

Method	**Spearman Correlation**	**Spearman p-value**	**Effect Estimate**	**Effect Standard Error**	**Effect t-value**	**Effect p-value**
Bisque	-0.178	0.090	-0.282	0.126	-2.240	**0.030**
MuSiC	0.038	0.719	-0.081	0.108	-0.754	0.455
BSEQ-sc	-	-	-	-	-	-
CIBERSORT	-	-	-	-	-	-
CIBERSORTx	-0.295	**0.005**	-0.355	0.102	-3.478	**0.001**
BisqueMarker	-0.227	**0.030**	-0.304	0.096	-3.154	**0.003**

b Association of macrophage proportion estimates in adipose tissue with BMI

Method	**Spearman Correlation**	**Spearman p-value**	**Effect Estimate**	**Effect Standard Error**	**Effect t-value**	**Effect p-value**
Bisque	0.389	$<$ **0.001**	0.460	0.099	4.671	$<$ **0.001**
MuSiC	0.065	0.540	0.034	0.110	0.308	0.760
BSEQ-sc	0.238	**0.022**	0.278	0.092	3.301	**0.004**
CIBERSORT	0.239	**0.022**	0.162	0.102	1.597	0.118
CIBERSORTx	0.283	**0.007**	0.212	0.104	2.029	**0.049**
BisqueMarker	0.296	**0.004**	0.253	0.103	2.465	**0.018**

c Association of T cell proportion estimates in adipose tissue with Matsuda index

Method	**Spearman Correlation**	**Spearman p-value**	**Effect Estimate**	**Effect Standard Error**	**Effect t-value**	**Effect p-value**
Bisque	-0.195	0.075	-0.287	0.116	-3.328	$<$ **0.001**
MuSiC	-	-	-	-	-	-
BSEQ-sc	-	-	-	-	-	-
CIBERSORT	-	-	-	-	-	-
CIBERSORTx	-0.311	**0.004**	-0.230	0.111	-2.060	**0.047**
BisqueMarker	-0.294	**0.007**	-0.304	0.096	-3.154	**0.003**

Supplementary Table 1: Significance of associations of estimated cell proportions and measured phenotypes in 100 subcutaneous adipose tissue samples. We fit a linear mixed-effects model (LMM) to account for the twin structure of the dataset as a random effect, with additional fixed effects to account for age, age-squared, and sex. Expected effect directions were based on previously reported findings. An entry of '-' indicates that the method did not detect the indicated cell population in any of the samples. Bold values were found to be significant at $\alpha = 0.05$ and in expected directions.
a Association of adipocyte proportion with BMI. A negative association was expected.
b Association of macrophage proportion with BMI. A positive association was expected.
c Association of T cell proportion with Matusda index, a measure of insulin resistance. A negative association was expected. An additional covariate accounting for diabetes status was added to the LMM due to previously reported significant associations with Matsuda index.

a Association of neuron proportion estimates in DLPFC tissue with cognitive diagnosis

Method	**Spearman Correlation**	**Spearman p-value**	**Effect Estimate**	**Effect Standard Error**	**Effect t-value**	**Effect p-value**
Bisque	-0.167	< **0.001**	-0.115	0.039	-2.950	**0.003**
MuSiC	-0.167	< **0.001**	-0.123	0.039	-3.155	**0.002**
BSEQ-sc	-0.142	< **0.001**	0.018	0.039	0.465	0.642
CIBERSORT	-0.173	< **0.001**	-0.116	0.039	-2.965	**0.003**
CIBERSORTx	-0.162	< **0.001**	-0.137	0.039	-3.517	< **0.001**
BisqueMarker	-0.141	< **0.001**	-0.121	0.039	-3.098	**0.002**

b Association of microglia proportion estimates in DLPFC tissue with Braak stage

Method	**Spearman Correlation**	**Spearman p-value**	**Effect Estimate**	**Effect Standard Error**	**Effect t-value**	**Effect p-value**
Bisque	0.094	**0.018**	0.118	0.037	3.220	**0.001**
MuSiC	0.057	0.151	0.019	0.037	0.509	0.611
BSEQ-sc	-0.190	< 0.001	-0.166	0.037	-4.525	< 0.001
CIBERSORT	0.003	0.943	-0.005	0.037	-0.137	0.891
CIBERSORTx	0.109	**0.006**	0.056	0.037	1.517	0.130
BisqueMarker	0.092	**0.021**	0.054	0.037	1.444	0.149

Supplementary Table 2: Significance of associations of estimated cell proportions and measured phenotypes in DLPFC tissue. We fit a linear model with covariates to account for age, age-squared, and sex. Expected effect directions were based on previously reported findings. Bold values were found to be significant at $\alpha = 0.05$ and in expected directions.
a Association of neuron proportion with cognitive diagnosis category. A negative association was expected.
b Association of microglia proportion with Braak stage, a measure of neurofibrillary tangles. A positive association was expected.

Figures

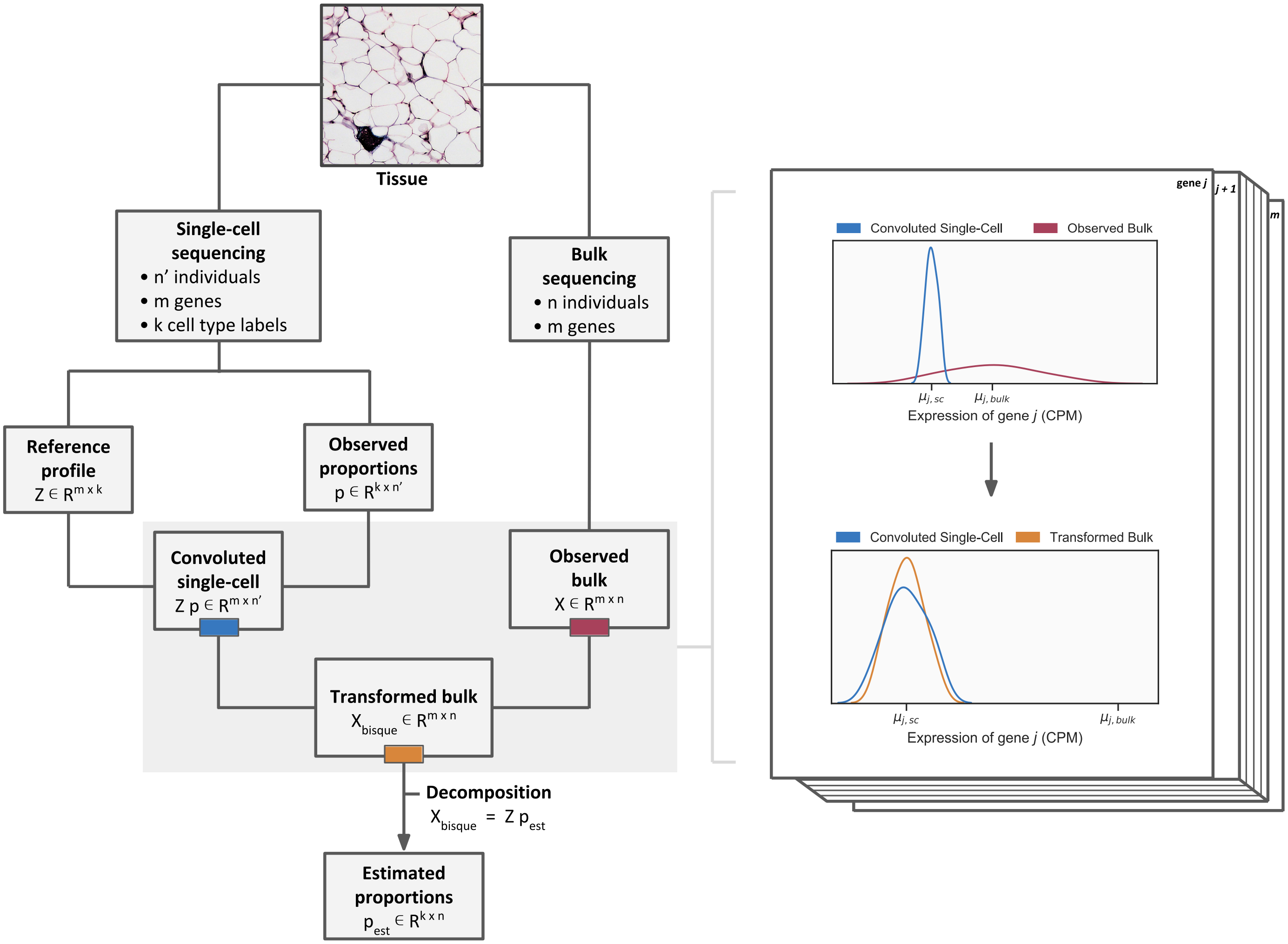

Figure 1: Graphical overview of the Bisque decomposition method. We integrate single-cell and bulk expression by learning gene-specific bulk transformations (pictured on right) that align the two datasets for accurate decomposition.

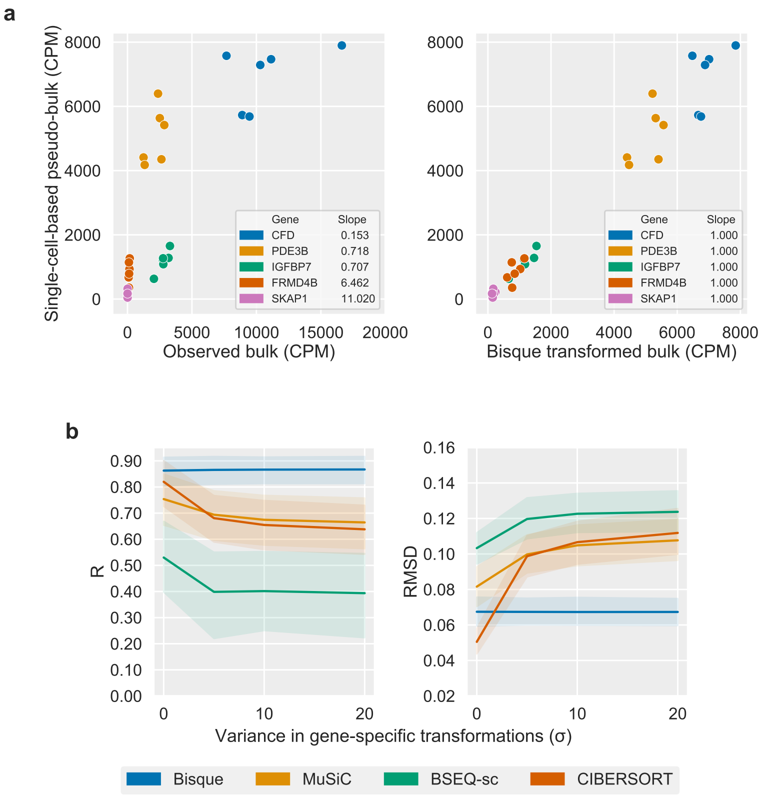

Figure 2: The effect of discrepancies between a single-cell based reference and bulk expression on decomposition. **a** Observed discrepancies in real data between single-nucleus and bulk expression for selected marker genes (left) for six individuals. Each color corresponds to a gene. On the left, observed bulk expression on the x-axis is plotted against the pseudo-bulk expression on the y-axis, where pseudo-bulk expression is calculated by summing the single-cell based reference with cell proportions as weights. On the right, the Bisque transformation of bulk expression is on the x-axis. Bisque recovers a one-to-one relationship by transforming the bulk expression for improved decomposition accuracy (right).
b Simulation of bulk expression for six individuals based on true adipose snRNA-seq data with increasing gene-specific differences. These differences are modeled as a linear transformation of the summed snRNA-seq counts with coefficient and intercept sampled from Half-Normal distributions with parameter as indicated on the x-axis. At $\sigma = 0$, the simulated bulk is simply the sum of the observed single-cell read counts. Performance on y-axis measured in global Pearson correlation (R) (left) and root mean squared deviation (RMSD) (right). Shaded regions indicate 95% confidence intervals based on bootstrapping. Bisque remains robust to increasing gene-specific variation between single-cell and bulk expression levels.

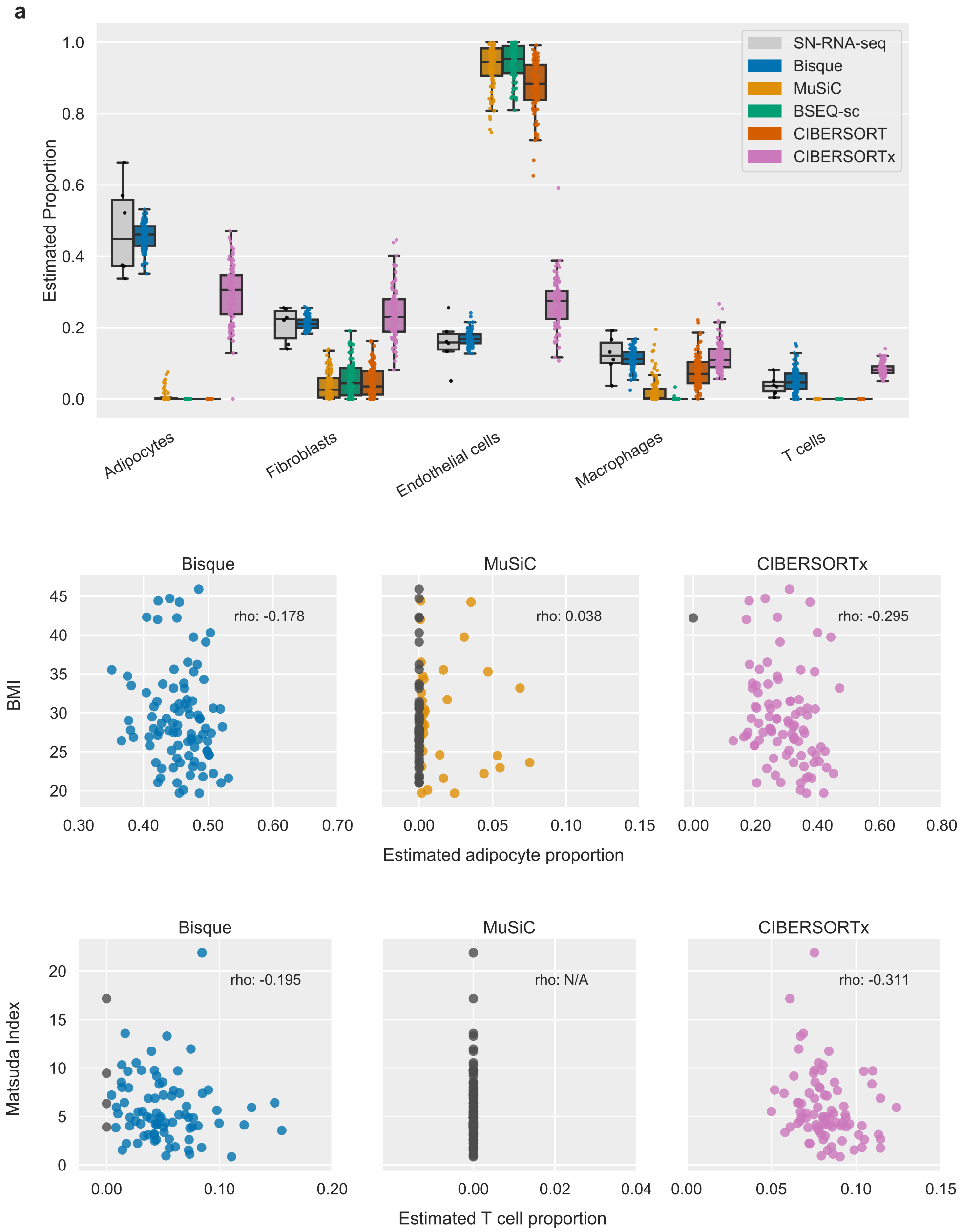

Figure 3: Decomposition benchmark in human subcutaneous adipose tissue.
a Comparison of decomposition estimates from 100 individuals with estimates from 6 individuals with snRNA-seq data available. Each color represents a benchmarked method.
b-c Scatterplots comparing decomposition estimates with measured phenotypes in 100 individuals. Reported ‘rho’ corresponds to Spearman correlation. CIBERSORT and BSEQ-sc are not shown since they did not detect these cell populations. These examples include the most abundant (adipocytes) and rarest (T cells) cell types identified in the snRNA-seq data. Significance of associations reported in Supplementary Table 1.
b Adipocyte proportion has been observed to negatively correlate with BMI so we expected a negative correlation. Bisque ($p = 0.030$) and CIBERSORTx ($p = 0.001$) produced significant negative associations after correcting for sex, age, age-squared, and relatedness.
c T cell proportion has previously been reported to positively correlate with insulin resistance. Matsuda index decreases with higher insulin resistance so we expected a negative correlation. Bisque ($p < 0.001$) and CIBERSORTx ($p = 0.003$) produced significant negative associations after correcting for diabetes status, sex, age, age-squared, and relatedness.

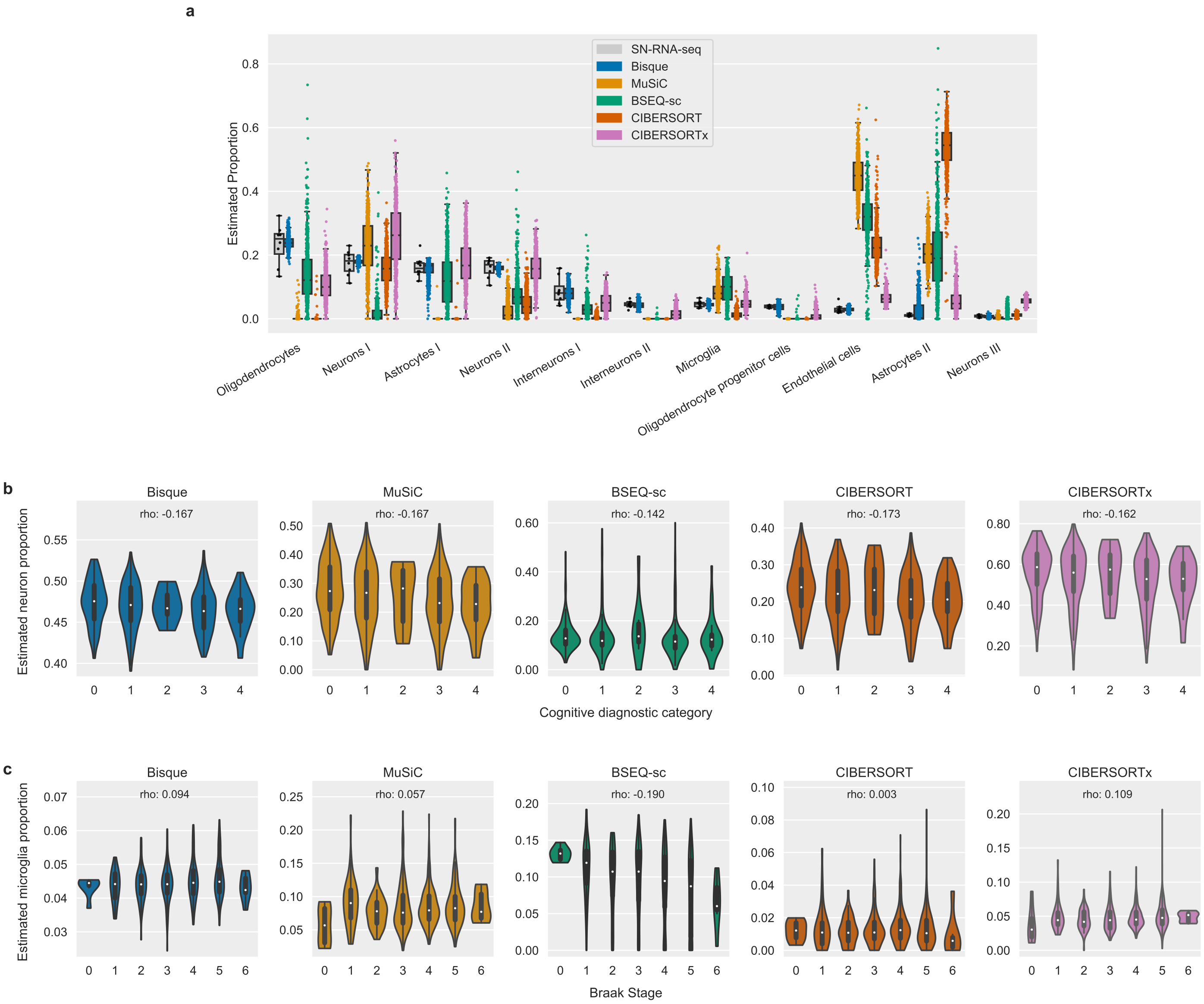

Figure 4: Decomposition benchmark in human dorsolateral prefrontal cortex tissue. We randomly sampled 25% of the nuclei in the snRNA-seq data to accommodate the file size limit of the web-based implementation of CIBERSORTx at the time of writing.

a Comparison of decomposition estimates from 628 individuals with estimates from 8 individuals with snRNA-seq data available. Each color represents a benchmarked method.

b-c Violin plots depicting association of decomposition estimates aggregated into major cell types with measured phenotypes in 628 individuals. Reported 'rho' corresponds to Spearman correlation. Examples shown are for the most abundant (neurons) and least abundant (microglia) populations detected in the snRNA-seq data. Significance of associations reported in Supplementary Table 2.

b Neuronal degeneration has been observed in patients diagnosed with Alzheimer's disease (AD). Cognitive diagnostic category measures a physician's diagnosis of cognitive impairment (CI), with 0 indicating no CI and 4 indicating a confident AD diagnosis. We expected a negative correlation between neuron proportion and cognitive diagnostic category.

c Microglia proportion has been observed to positively correlate with increased severity of AD symptoms, such as neurofibrillary tangles. Braak stage provides a semiquantitative measure of tangle severity, so we expected an overall positive correlation between microglia proportion and Braak stage. In addition, a decrease in microglia abundance has been previously reported at Braak stages 5 through 6 in AD patients. Only Bisque produced estimates with a significant positive association ($p = 0.001$) after correcting for sex, age, and age-squared.

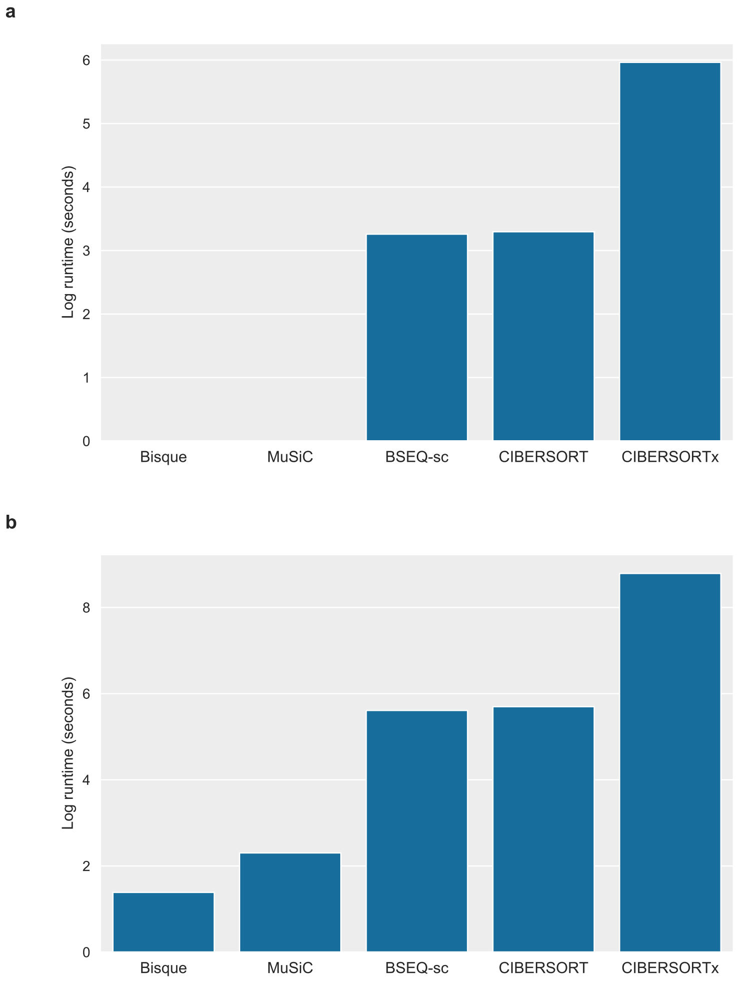

Figure 5: Runtime comparisons in log-transformed seconds for benchmarked reference-based decomposition methods.

a Runtime for subcutaneous adipose dataset, which included 100 RNA-seq samples and 6 snRNA-seq samples with around 1,800 nuclei per individual.

b Runtime for dorsolateral prefrontal cortex dataset, which included 628 RNA-seq samples and 8 snRNA-seq samples. We benchmarked each method using around 2,125 nuclei per snRNA-seq sample.

Supplementary Figures

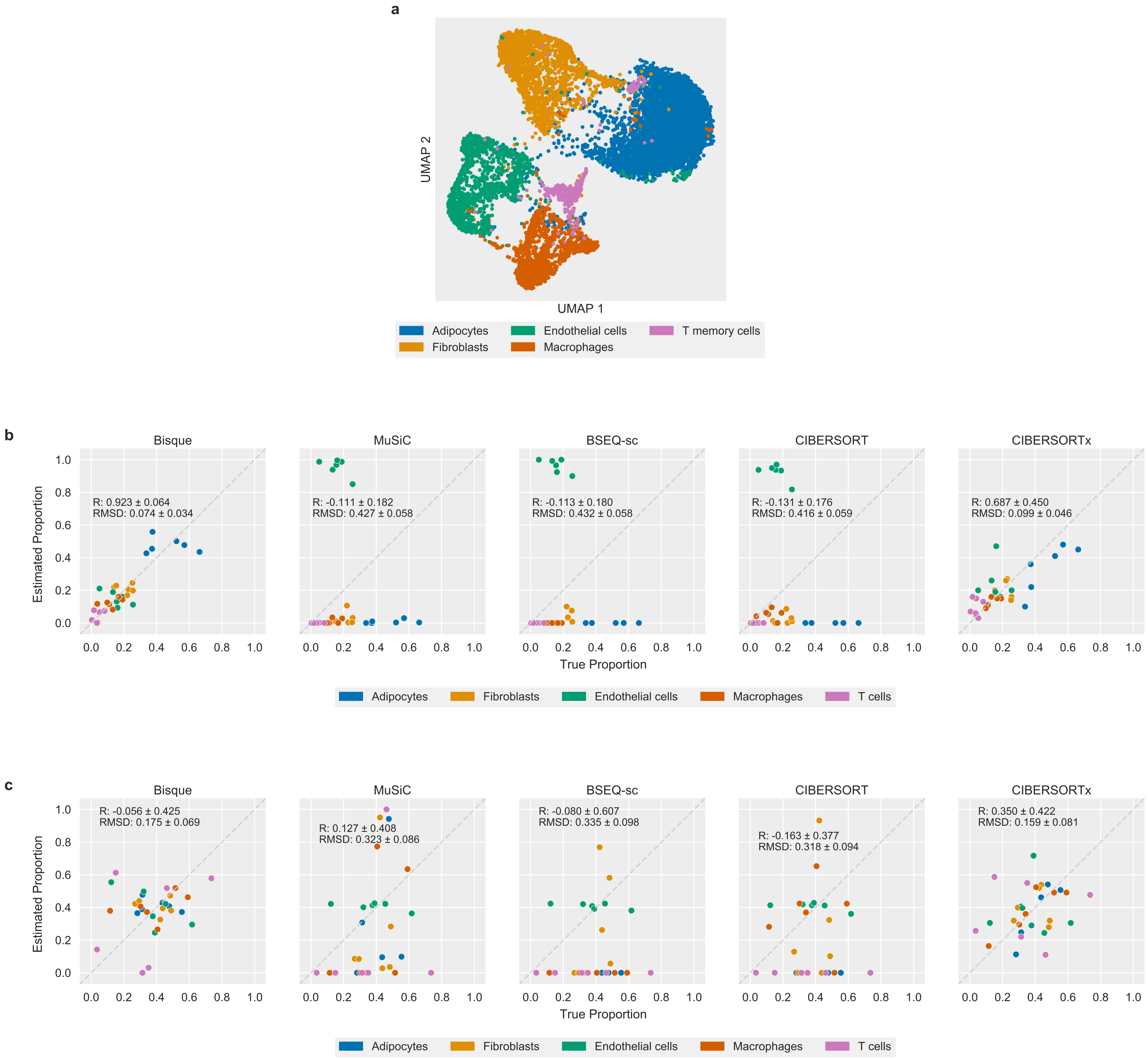

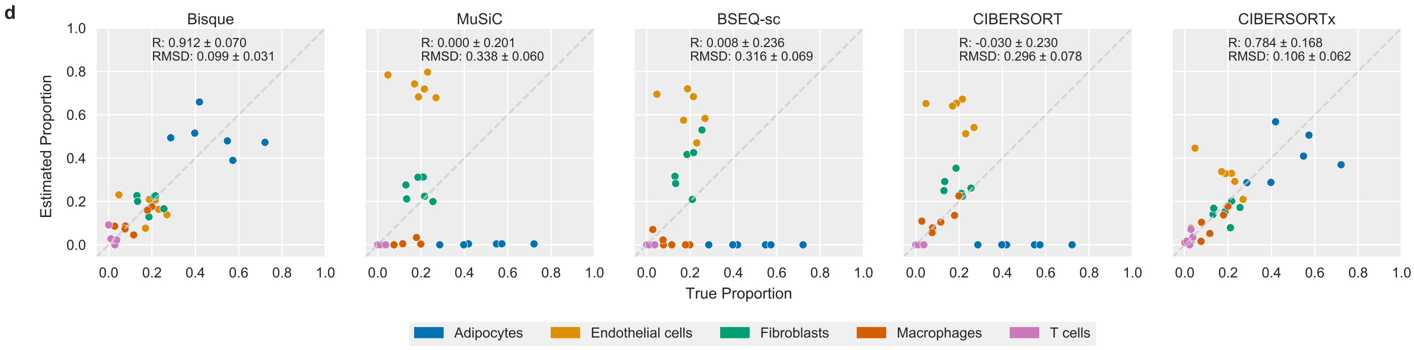

Supplementary Figure 1: Decomposition of human subcutaneous adipose tissue.
a UMAP projection of snRNA-seq data with 5 identified cell type clusters labeled.
b Leave-one-out cross-validation using 6 samples with snRNA-seq and bulk RNA-seq data available. Proportions based on snRNA-seq were used as a proxy for the true proportions on the x-axis. Estimated proportions for an individual were generated by each decomposition method using the remaining 5 individuals as training data. Each color represents one of the 5 identified cell populations.
c Leave-one-out cross-validation performance after normalization of estimates within each cell type to determine cell-specific accuracy. Normalized estimates are robust to inflation of global Pearson correlation by large cell populations; however, these metrics are noisy when considering only six individuals.
d Leave-one-out cross-validation performance on exon-aligned snRNA-seq data. Existing methods are able to detect additional cell populations using the exonic subset of the snRNA-seq data, though around 40% of the sequenced cells are filtered out.

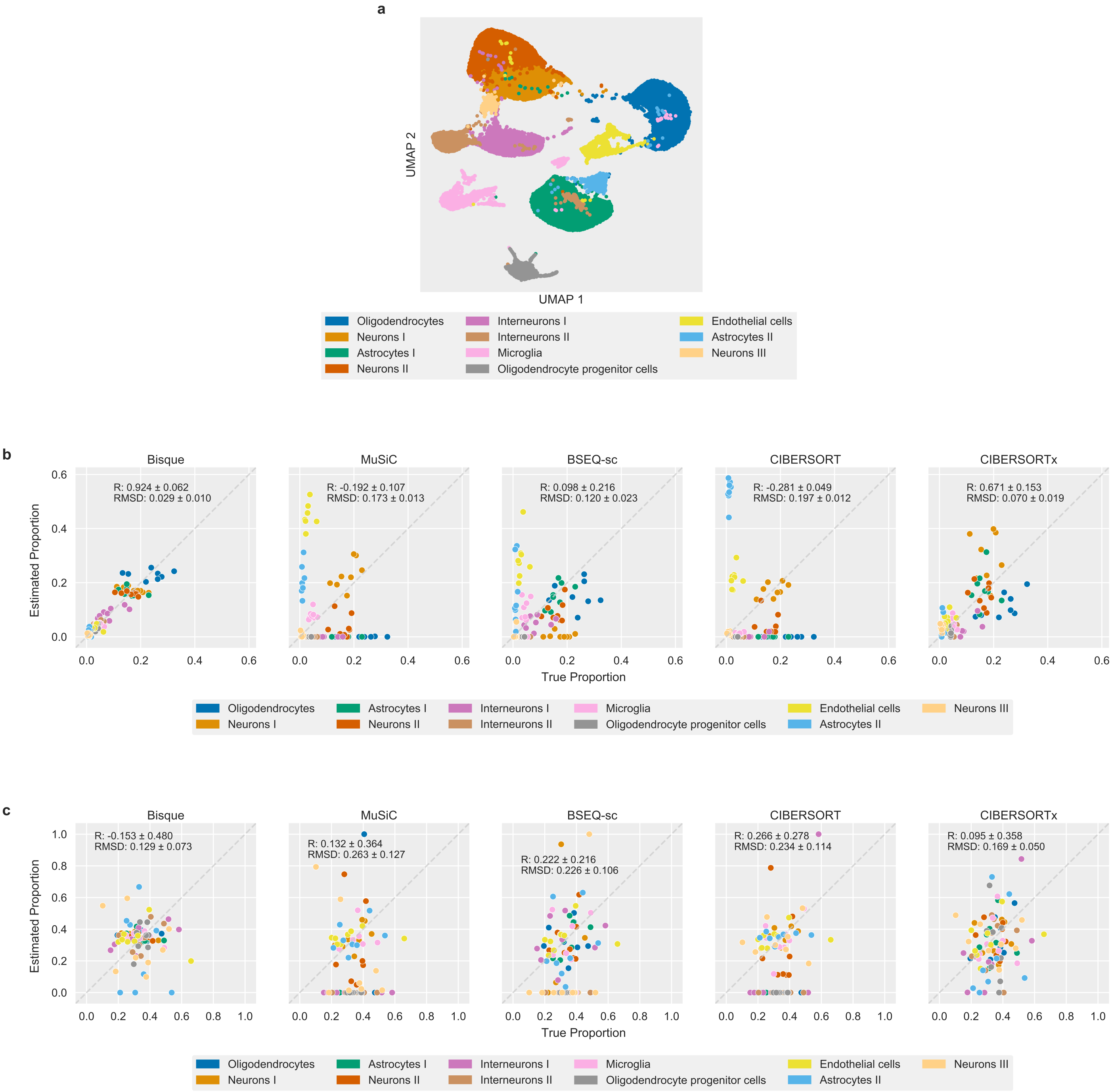
a
UMAP 2
UMAP 1
Oligodendrocytes
Neurons I
Astrocytes I
Neurons II
Interneurons I
Interneurons II
Microglia
Oligodendrocyte progenitor cells
Endothelial cells
Astrocytes II
Neurons III
b
Bisque
MuSiC
BSEQ-sc
CIBERSORT
CIBERSORTx
Estimated Proportion
True Proportion
R: 0.924 ± 0.062
RMSD: 0.029 ± 0.010
R: -0.192 ± 0.107
RMSD: 0.173 ± 0.013
R: 0.098 ± 0.216
RMSD: 0.120 ± 0.023
R: -0.281 ± 0.049
RMSD: 0.197 ± 0.012
R: 0.671 ± 0.153
RMSD: 0.070 ± 0.019
0.0
0.2
0.4
0.6
Oligodendrocytes
Neurons I
Astrocytes I
Neurons II
Interneurons I
Interneurons II
Microglia
Oligodendrocyte progenitor cells
Endothelial cells
Astrocytes II
Neurons III
c
Bisque
MuSiC
BSEQ-sc
CIBERSORT
CIBERSORTx
Estimated Proportion
True Proportion
R: -0.153 ± 0.480
RMSD: 0.129 ± 0.073
R: 0.132 ± 0.364
RMSD: 0.263 ± 0.127
R: 0.222 ± 0.216
RMSD: 0.226 ± 0.106
R: 0.266 ± 0.278
RMSD: 0.234 ± 0.114
R: 0.095 ± 0.358
RMSD: 0.169 ± 0.050
0.0
0.2
0.4
0.6
0.8
1.0
Oligodendrocytes
Neurons I
Astrocytes I
Neurons II
Interneurons I
Interneurons II
Microglia
Oligodendrocyte progenitor cells
Endothelial cells
Astrocytes II
Neurons III

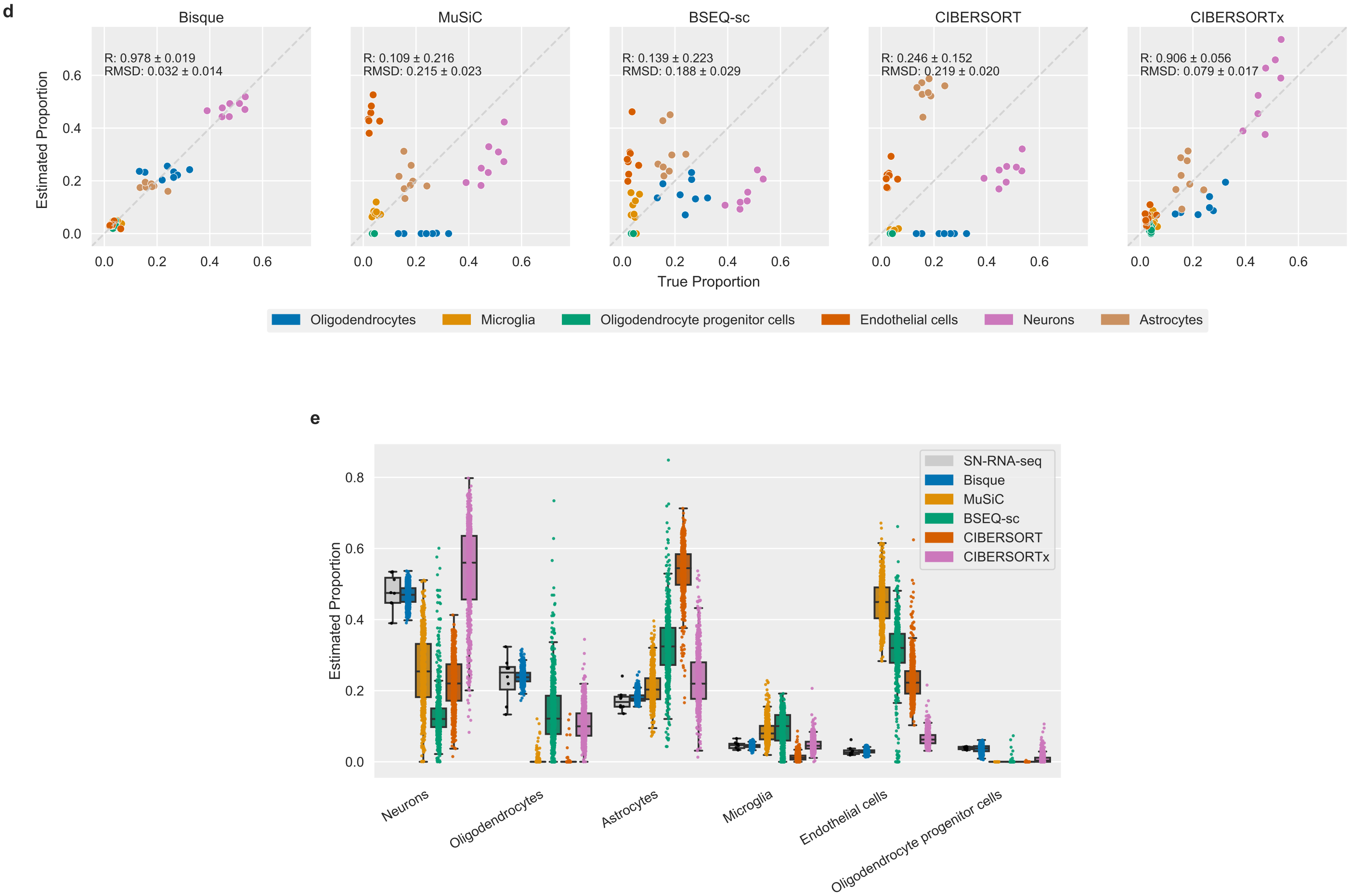

Supplementary Figure 2: Decomposition of human DLPFC tissue.

a UMAP projection of snRNA-seq data with 11 identified cell type clusters labeled.

b Leave-one-out cross validation using 8 samples with snRNA-seq and bulk RNA-seq data available. Proportions based on snRNA-seq were used as a proxy for the true proportions on the x-axis. Estimated proportions for an individual were generated by each decomposition method using the remaining 7 individuals as training data. Each color represents one of the 11 identified cell populations.

c Leave-one-out cross-validation performance after normalization of estimates within each cell type to determine cell-specific accuracy. As described previously, performance metrics on normalized data provide better measure of global accuracy but are noisy with small sample sizes.

d Leave-one-out cross-validation performance after merging closely related cell subtypes into 6 clusters. Performance of existing methods increases compared to decomposition into 11 clusters with related subtypes.

e Decomposition of remaining 628 individuals with cell subtype merging. The aggregated cell type proportions estimated from the 8 snRNA-seq samples are similar to IHC estimates for neurons and astrocytes from 70 individuals in the cohort (data not shown).

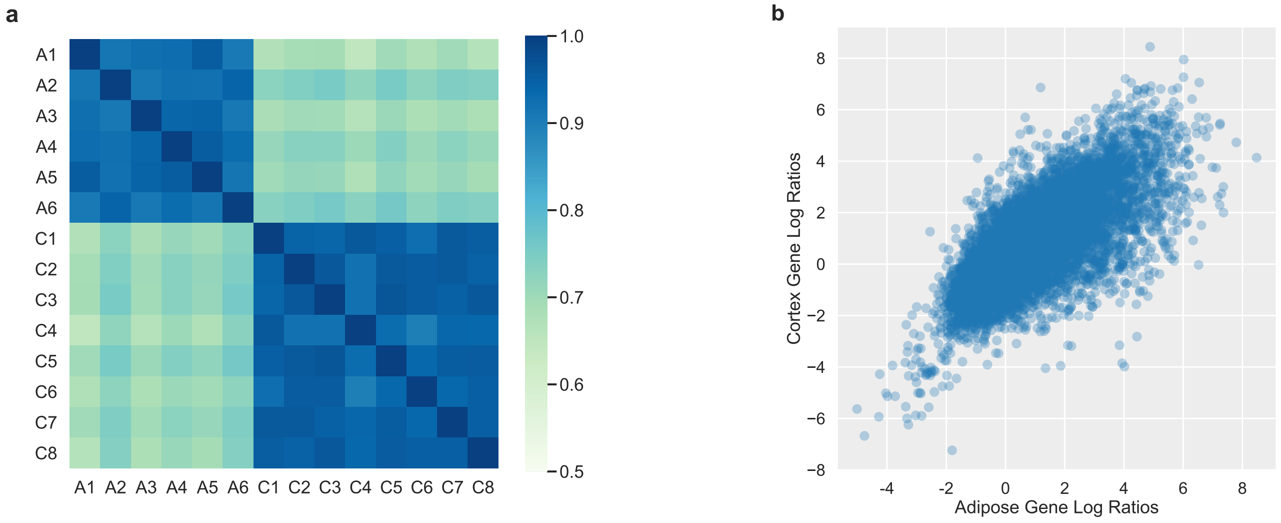

Supplementary Figure 3: Consistency of snRNA-seq to bulk RNA-seq expression log-ratios across individuals, tissues, and experiments.
a Heatmap depicting Pearson correlation between pairs of individual's log-ratios of snRNA-seq expression to bulk RNA-seq gene expression measured in counts per million (CPM). A sample prefix of 'A' indicates an individual from the adipose dataset and 'C' indicates an individual from the cortex dataset. Correlation is high between individuals within experiments as well as between experiments/tissues, indicating the same genes are over/under-expressed in snRNA-seq when compared to bulk RNA-seq.
b Scatterplot of average snRNA-seq to bulk RNA-seq gene expression log-ratios across individuals in adipose dataset (x-axis) and cortex dataset (y-axis). Each point corresponds to a gene detected in both experiments, depicting the average ratio across all individuals for that tissue. The snRNA-seq to bulk RNA-seq ratios vary across genes and correlate (R=0.747) between these two experiments.

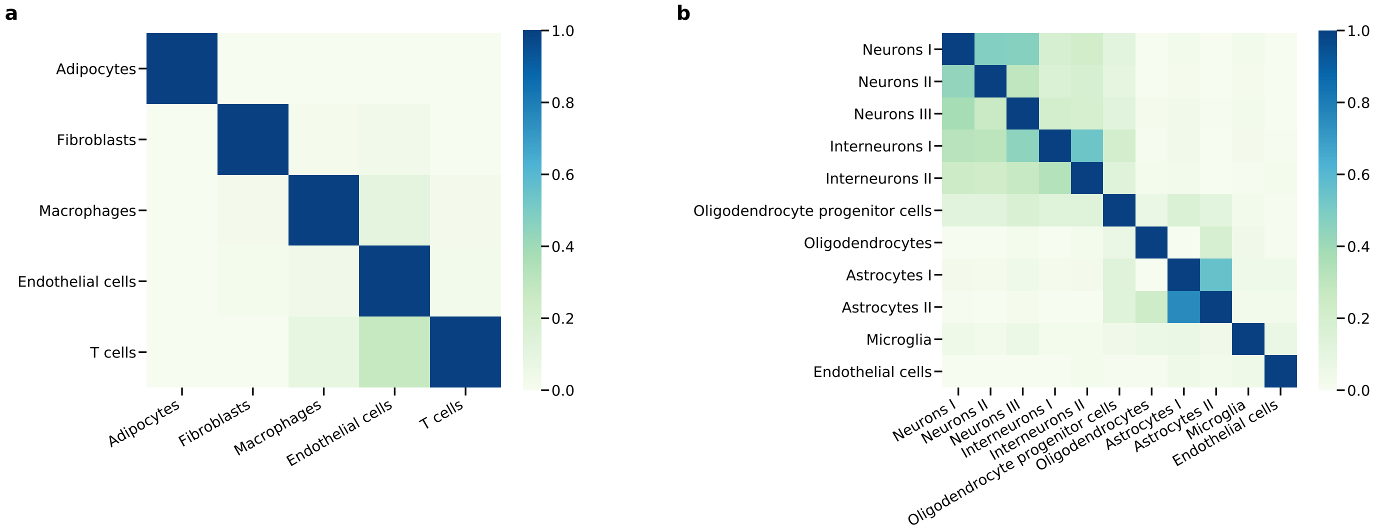

Supplementary Figure 4: Shared marker genes between identified clusters in snRNA-seq data. Heatmaps of proportion of shared marker genes where an entry indicates the proportion of marker genes for the cluster on the x-axis that are found in the cluster on the y-axis.
a The 5 clusters identified in adipose tissue are relatively distinct in their marker genes.
b The 11 clusters identified in DLPFC tissue have several closely related subtypes, such as neurons and astrocytes.